Journal of Alloys and Compounds 896 (2021) 163010

Contents lists available at ScienceDirect

Journal of Alloys and Compounds

journal homepage: www.elsevier.com/locate/jalcom

Efficient synthesis of high areal capacity Si@graphite@SiC composite anode material via one-step electro-deoxidation

Jong-Hyeok Choi[a,1], Sunghun Choi[b,1], Jung Sang Cho[c], Hyun-Kyung Kim[d,e,*], Sang Mun Jeong[a,**]

[a] Department of Chemical Engineering, Chungbuk National University, 1 Chungdea-ro Heungduk-gu, Cheongju 28644, Republic of Korea
[b] Gwangju Bio/Energy R&D Center, Korea Institute of Energy Research (KIER), 270-25 Samso-ro, Buk-gu, Gwangju 61003, Republic of Korea
[c] Department of Engineering Chemistry, Chungbuk National University, 1 Chungdea-ro Heungduk-gu, Cheongju 28644, Republic of Korea
[d] Department of Materials Science and Engineering, Kangwon National University, Chuncheon 24341, Republic of Korea
[e] Interdisciplinary Program in Advanced Functional Materials and Devices Development, Kangwon National University, Chuncheon 24341, Republic of Korea

ARTICLE INFO

Article history:
Received 15 July 2021
Received in revised form 3 November 2021
Accepted 26 November 2021
Available online 28 November 2021

Keywords:
Molten salt
Electro-deoxidation
Energy storage materials
Si@graphite@SiC composite
Lithium-ion batteries

ABSTRACT

Although Si is a promising anode material for lithium-ion batteries, scalable synthesis of Si anodes with high cyclability and low swelling remains a significant challenge. Herein, we describe the electrochemical fabrication of a Si@graphite@SiC composite anode from a SiO_2/graphite mixture via an electro-deoxidation-based molten salt process. The exfoliated graphite enhances the electrical conductivity of the composite and cushions the volume expansion of Si nanowires, while the SiC component acts as an active matrix that accommodates the expansion of the Si during lithiation. This significantly increases the electrode cycle life. In half-cell testing, the composite exhibited 80% capacity retention until 500 cycles. It showed good cycling performance even at a high areal capacity of 4.6 mAh/cm^2. Further, a full cell comprising the composite anode and a $LiNi_{0.6}Co_{0.2}Mn_{0.2}O_2$ cathode possessed a high capacity and demonstrated 84% capacity retention after 70 cycles. This work provides new insights into the rational design of alloy anodes for high-energy density batteries.

1. Introduction

Global demand for Lithium-ion batteries (LIBs), ranging from small batteries embedded in wireless earbuds in wireless earbuds to ultra-high capacity batteries is rapidly increasing, due to its own high gravimetric and volumetric energy densities compared to other secondary battery systems and supercapacitor [1–5]. Conventional graphite anodes for LIBs have a low theoretical specific capacity of 372 mAh g^{-1} and are rapidly reaching their energy limit; these necessitate the development of new high-performance anode electrode materials [1]. Si anodes have attracted considerable research interest owing to their high specific capacity (3579 mAh g^{-1}) and low lithiation voltage plateau (vs. Li/Li$^+$); however, the commercialisation of these electrodes is impeded by several issues, many of which can be attributed to the volume expansion that occurs during the lithiation process [6–8]. These issues have been recently addressed via the development of various nano-structural morphologies and coatings that can effectively accommodate the volume expansion of Si electrodes and increase their cycle life [9–13]. However, despite these advancements, other problems related to the use of Si nano-structured electrodes remain unsolved. In particular, such electrodes undergo intense side reactions due to their large surface areas, resulting in a low Coulombic efficiency (CE). The small particle size increases the inter-particle free volume and surface area, which lowers the tap density and increases the inter-particle resistance [14–17]. Moreover, the low tap density increases the electrode thickness and creates longer electron transfer channels that hamper the achievement of high areal capacity [12].

To mitigate the aforementioned drawbacks, several research groups have successfully developed advanced nano-/micro-designing strategies combined with the application of carbon materials. These include Si–C yolk–shell and pomegranate structures as well as core–shell fibres [14,15,18–24]. Recently, the structural

* Corresponding author at: Department of Materials Science and Engineering, Kangwon National University, Chuncheon 24341, Republic of Korea
** Corresponding author.
E-mail addresses: hkk@kangwon.ac.kr (H.-K. Kim), smjeong@chungbuk.ac.kr (S.M. Jeong).
[1] These authors (J.-H.C. and S. C.) contributed equally to this work.

https://doi.org/10.1016/j.jallcom.2021.163010
0925-8388/

design of well-dispersed Si NPs embedded in a micron-sized carbon buffer has drawn attention owing to the excellent electrochemical performance of such NPs [25,26]. However, most despite the successful preparation of Si–C composite electrodes, some fundamental barriers prevent their large-scale implementation in LIBs. For instance, the commercially available carbon nanomaterials, such as graphene and carbon nanotubes, with superior electrochemical performance are at least ten times more expensive than graphite [18,19]. Moreover, the appropriate synthesis routes of nano/micro Si–C composites, including chemical vapour deposition, electrospinning, and multi-step etching, involve high manufacturing costs, potentially hazardous precursors, and low yields. In fact, the cost of manufacturing SiH_4 via chemical vapour deposition exceeds 100 USD kg^{-1}, which translates to hundreds of dollars per kilogram of Si–C powder [12,27–29].

To overcome these disadvantages, some researchers have considered the Fray–Farthing–Chen (FFC) Cambridge process, which is a facile and economical method for direct extraction of high-purity metals and alloys via the electro-deoxidation of the cathode material in molten salt [30,31]. It can be modified for the synthesis of metal carbides by employing cathode materials that consist of metal oxides and carbon and by optimising the reaction conditions, such as applied voltage and electrolysis time [32–35]. Several recent studies have demonstrated the successful application of the FFC Cambridge process to synthesise anode materials such as carbonised rice husks [36] and Si@carbon composites [37,38] via direct electrolysis in molten $CaCl_2$. However, the majority of synthesis methods involving molten salt electrolysis still pose considerable challenges and require multiple processing steps, which may hinder the application of these methods in large-scale commercial production of anode materials.

In this study, we synthesised Si@graphite@SiC composite anode materials through a one-step molten salt electrolysis method (FFC Cambridge process) and performed a detailed analysis of the electro-deoxidation mechanism of the SiO_2/graphite mixture. Further, we first evaluated the potential commercial utilisation of these materials by fabricating full cells containing commercial cathode Si@carbon composites via direct electrolysis in molten $CaCl_2$ [30,31]. In the composite fabrication procedure, Si nanowires (NWs) were grown in situ on the graphite surface with SiC connections, which enhanced the cycling performance owing to their robust and electrically conducting buffer matrix even at a high areal capacity (4.6 mAh/cm^2) [39]. Considering that a part of the surface of Si NWS was transformed into SiC, the SiC coating could accommodate repeated huge volume changes in inner Si NWs owing to its high mechanical strength and play a key role in forming a stable SEI layer [40]. The Si@graphite@SiC nano-/micro-structure demonstrated good processability and excellent electrochemical performance. The electrode with a high mass loading of approximately 3.5 mg cm^{-2} exhibited outstanding electrochemical properties corresponding to a maximum discharge capacity of 4.6 mAh cm^{-2}, confirming its favourable electron transfer characteristics and stable structure. Furthermore, the full cell, containing the composite anode and a $LiNi_{0.6}Co_{0.6}Mn_{0.2}O_2$ (NCM622) cathode, possessed a high capacity of 130 mAh g^{-1} with a charging and discharging rate of 0.1 C (1 C = 180 mA g^{-1} based on the cathode active material) and demonstrated 84% capacity retention after 70 cycles. Therefore, this work provides new insights into the rational design of alloy anodes for high-energy batteries. Moreover, the proposed technology can open new avenues for the development of novel Si composite materials and synthesis of high-performance anode materials for LIBs.

2. Experimental section

2.1. Electro-deoxidation of SiO_2/graphite pellets

To synthesise SiO_2/graphite pellets, commercial SiO_2 (325 mesh, 99.5% purity, Aldrich) and graphite (particle size < 20 μm, Aldrich) powders were mixed at an atomic ratio of 1:1.5 in a mortar. The resulting mixture was converted into a slurry by adding 2-propanol (99.5% purity, SAMCHUN, South Korea), polyvinyl alcohol (PVA, M_w = 89,000–98,000, 99% hydrolysed, Aldrich), and zinc stearate (technical grade, Aldrich) binder and was ground in a ball mill at a speed of 400 rpm and dried at 80 °C for 24 h. The obtained powder with a weight of approximately 0.5 g was pressed at 6 MPa in a cylindrical mould (⌀13 mm) and sintered at 1000 °C in a N_2 atmosphere for 3 h to prepare a solid pellet for electro-deoxidation. Then, 500 g of anhydrous $CaCl_2$ (> 95.0% purity, Junsei, Japan) was pre-dried at 500 °C in air for 1 d. The dried $CaCl_2$ salt was heated to 850 °C in an alumina crucible (99% purity, ⌀80 mm) and periodically flushed with Ar inside a glove box filled with high-purity Ar.

To perform cyclic voltammetry (CV), a pinhole (⌀0.5 mm) was drilled in a Mo wire (99.95% purity, Alfa Aesar) and SiO_2/graphite powder was placed inside the pinhole to fabricate a working metallic cavity electrode (MCE). A Ag/AgCl electrode, consisting of Ag wire (99.99% purity, ⌀0.5 mm, Aldrich) immersed in molten $CaCl_2$ containing 1 M AgCl (99.5% purity, SAMCHUN, South Korea) in a mullite tube, was used as the reference electrode. A potentiostat (Autolab, PGSTAT362N) was used during the CV experiments, which were conducted at a fixed scan rate of 100 mV s^{-1}. The SiO_2/graphite pellets were wrapped in a Ni mesh (20 mesh woven from 0.18⌀ mm wire, Alfa Aesar) and Ni wire (⌀0.5 mm, Alfa Aesar) to prepare cathodes for the electro-deoxidation experiments. The Ni mesh and wire acted as the current lead, and a graphite rod (⌀1.27 cm, 99% purity, Alfa Aesar) was used as the anode. The electrolysis of the SiO_2/graphite pellets was performed by applying a cell voltage of 2.6–2.9 V from a DC power supply (E3633A, Agilent) for 5–15 h. A multimeter (34401A, Agilent) was used to continuously monitor the cathode potential during the electrolysis. After electrolysis, the cathode product (Si@graphite@SiC powder) was removed from the cell, washed with deionised water, and soaked in 0.1 M HCl solution (SAMCHUN, South Korea). The produced Si@graphite@SiC powder was sintered at 1000 °C in N_2 atmosphere for 3 h.

2.2. Cell preparation and electrochemical characterisation

The electrochemical properties of the fabricated electrodes were tested in CR-2032 type coin cells assembled inside an Ar-filled glove box (99.99% purity). The electrolyte consisted of 1.15 M $LiPF_6$ solution in a mixture of ethylene carbonate and dimethyl carbonate with a 3:7 vol ratio containing 10% fluorinated ethylene carbonate. A microporous membrane (Celgard 2400) was used as the separator for all the coin cells.

To perform half-cell tests, slurries were prepared by dissolving 70 wt% active materials, 15 wt% super P (> 99% purity, Alfa Aesar), and 15 wt% poly(acrylic) acid (M_w ≈ 100,000; 35 wt% in H_2O; Aldrich) in distilled water, which were then cast onto a Cu current collector via doctor blade technique in the mass loading range of 0.6–3.49 mg cm^{-2}. After drying at 80 °C in air, the electrode was pressed to 80% of its original thickness using a roll press (MSK-HRP-01, MTI) and then vacuum-dried at 120 °C for 5 h. Coin cells were assembled by pairing the working electrode with a piece of Li, which was used as the counter electrode. Galvanostatic charge-discharge (GCD) cycling tests (WBCS3000L, Wonatech) were performed in a voltage range from 0.01 to 2.0 V (vs. Li^+/Li) at a specific current of 0.05–6.0 A g^{-1} (the first two cycles were performed at 0.1 A g^{-1}). The areal capacities were obtained by dividing the measured cell capacity by the geometric area (2.0 cm^2), and cycling tests were

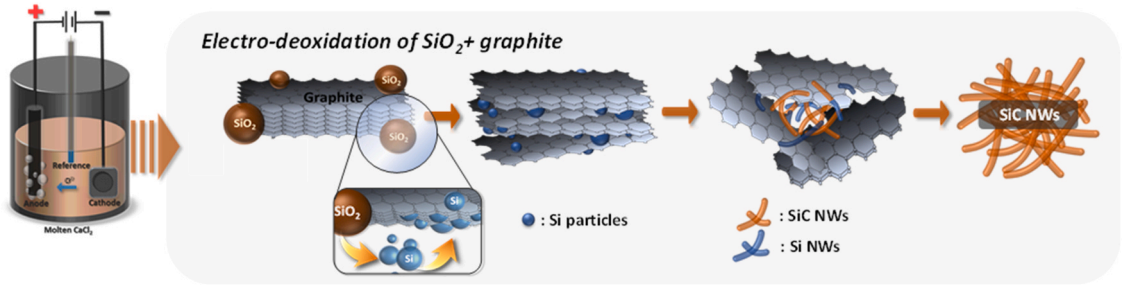

Fig. 1. Schematic illustration of the structural changes that occur during the electro-deoxidation of a Si/graphite mixture in molten $CaCl_2$.

conducted at a current density of 0.4 A cm^{-2} (the first two cycles were performed at 0.1 A cm^{-2}). Full cells were assembled by employing the Si@graphite@SiC composite, electrolysed at 2.9 V for 5 h, as the anode and a commercial NCM622 electrode as the cathode. The ratio between the areal capacities of the negative and positive electrodes was approximately 1.2:1. GCD cycling was performed to evaluate the electrochemical performance of the cells between 2.8 and 4.25 V at rates of 0.1–0.25 C. All full cells were charged at a constant current until the voltage reached 4.25 V and then constantly maintained at 4.25 V until the current dropped below 1/10 that of the constant current value. After that, the full-cells discharged the same current under CC mode until the voltage reached 2.80 V.

The morphologies of the samples were characterised by field-emission scanning electron microscopy (FESEM, Ultra Plus-FESEM) and high-resolution transmission electron microscopy (HRTEM, Tecnai F20 UT). Elemental mapping was performed by TEM–energy-dispersive X-ray spectroscopy (EDS). In addition, X-ray photoelectron spectroscopy (XPS; PHI Quantera-II instrument, Ulvac-PHI) studies were conducted. The crystal structures were determined by X-ray diffraction (XRD) with Cu Kα radiation at a wavelength of 0.054 nm.

3. Results and discussion

The Si@graphite@SiC composite was synthesised by molten salt electrolysis of SiO_2/graphite mixtures, as illustrated in Fig. 1. The formation of SiC during the electro-deoxidation in molten $CaCl_2$ at 1123 K is described by the following equations:

$$SiO_2 + 4e^- \rightarrow Si + 2O^{2-} \ (E_{1123\,K} = -1{\cdot}05\ V\ vs{\cdot}Ag/AgCl) \quad (1)$$

$$Si + C \rightarrow SiC \quad (2)$$

During electrolysis, SiO_2 in the SiO_2/graphite mixture is converted to Si NWs, which grow in situ on the graphite surface. During the growth process, the silica species form a network structure on the graphite surface in molten salt. This network structure is subsequently broken during the reduction process. As the electro-deoxidation continues, SiC is partially formed via the reaction of Si and graphite and produces a Si@graphite@SiC composite (2.7–2.9 V, 5 h). Finally, only SiC species are generated at longer reaction times.

The described reactions were investigated via CV by using an MCE (Fig. 2a). A rapid cathodic current was detected near −1.8 V when Mo wire was used as the working electrode (black solid curve), indicating Ca deposition due to the sufficiently negative cathode potential. In the case of SiO_2 (red solid curve), the cathodic current started near −1.0 V, and the peak current was detected at −1.2 V. For the SiO_2/graphite mixture (blue dashed curve), the cathodic current originated at −1.0 V and peaked at −1.2 V, after which its magnitude remained constant. The close values of the cathodic currents, measured for SiO_2 and the SiO_2/graphite mixture at approximately −1.0 V, could be attributed to the SiO_2 reduction, as indicated by the theoretical reduction potential formula (1). In the case of the SiO_2/graphite system (blue dashed curve), a constant cathodic current was maintained owing to the high electrical conductivity of graphite. The increase in the electrical conductivity of the composite after graphite addition is expected to improve the reduction efficiency of SiO_2 during the electro-deoxidation process. In addition, a large anodic peak (both SiO_2 and SiO_2/graphite mixture) occurs at − 1.8 V owing to Ca dissolution. Because SiO_2/graphite mixture has high reduction efficiency owing to graphite, Ca deposition occurred, considering the several cathodic peaks [41]. Proportionally, more Ca dissolution occurred, and higher anodic peaks were observed and confirmed. Subsequently, the residual anodic peaks were determined to result from the re-oxidation of the reduced SiO_2.

The cathodic potentials that were measured at certified constant cell voltages (2.6, 2.7, and 2.9 V) during the electro-deoxidation equalled − 1.2, − 1.4, and − 1.6 V (vs. Ag/AgCl), respectively (Fig. S1), which are reasonable values considering that SiO_2 reduction began at − 1.0 V and Ca deposition occurred near − 1.8 V. In this work, electro-deoxidation was performed by varying the cell voltage and electrolysis time; hence, Fig. 2b displays the time–current plots obtained during the electro-deoxidation at cell voltages of 2.6, 2.7, and 2.9 V and electrolysis times of 5 and 15 h. As the applied cell voltage was increased, the current increased gradually and the colour of the generated powder became lighter.

Fig. 2c shows the XRD patterns of the samples produced under different electro-deoxidisation conditions. These XRD patterns can help elucidate various stages of the conversion of SiO_2/graphite mixture to pure SiC. (1) SiO_2 phase of the SiO_2/graphite mixture is first reduced to Si (JCPDS No. 27–1402) and temporarily forms a Si@graphite composite (2.6 V, 5 h). (2) As electro-deoxidation continues, SiC (JCPDS No. 29.1129) is partially formed by the reaction of Si and graphite and produce a Si@graphite@SiC composite (2.7–2.9 V; 5 h). (3) Finally, a single SiC phase is formed as the SiC production increases with increasing reaction time (2.9 V; 15 h).

These steps are confirmed by the XPS patterns presented in Fig. 2d and Fig. S2. At a voltage of 2.7 V and reaction time of 5 h, the peak detected at 99.4 eV represents the produced Si species, and the peak centred at 100.4 eV corresponds to the SiC phase. The peaks located at 101.5, 102.4, and 103.3 eV result from the surface oxidation of SiO_2 or Si, which were not reduced during the electrolytic reduction process. The XPS profiles of Si 2p could normally be split into 2p 1/2 (99 eV) and 2p 3/2 (100 eV), but the peak corresponding to Si 2p 1/2 was obscured by Si–C peak. At a voltage of 2.9 V and an electrolysis time of 5 h, the intensity of the SiC peak at 100.3 eV increases significantly [42]. Additionally, the C 1 s spectrum is deconvoluted into three peaks at 283.2, 285.1, and 287.8 eV, as shown in Fig. S2, which are ascribed to Si–C, C–C, and C–O, respectively [42]. At a voltage of 2.9 V and an electrolysis time of 5 h, the intensity of the SiC peak at 283.2 eV increases significantly. As the diffusion rate of Ca^{2+} in the molten salt is constant, the electrochemical reaction rate increases proportionally with the potential difference, which implies that the deoxidation reaction rate increases at higher voltages. The interaction of the product with the molten salt during

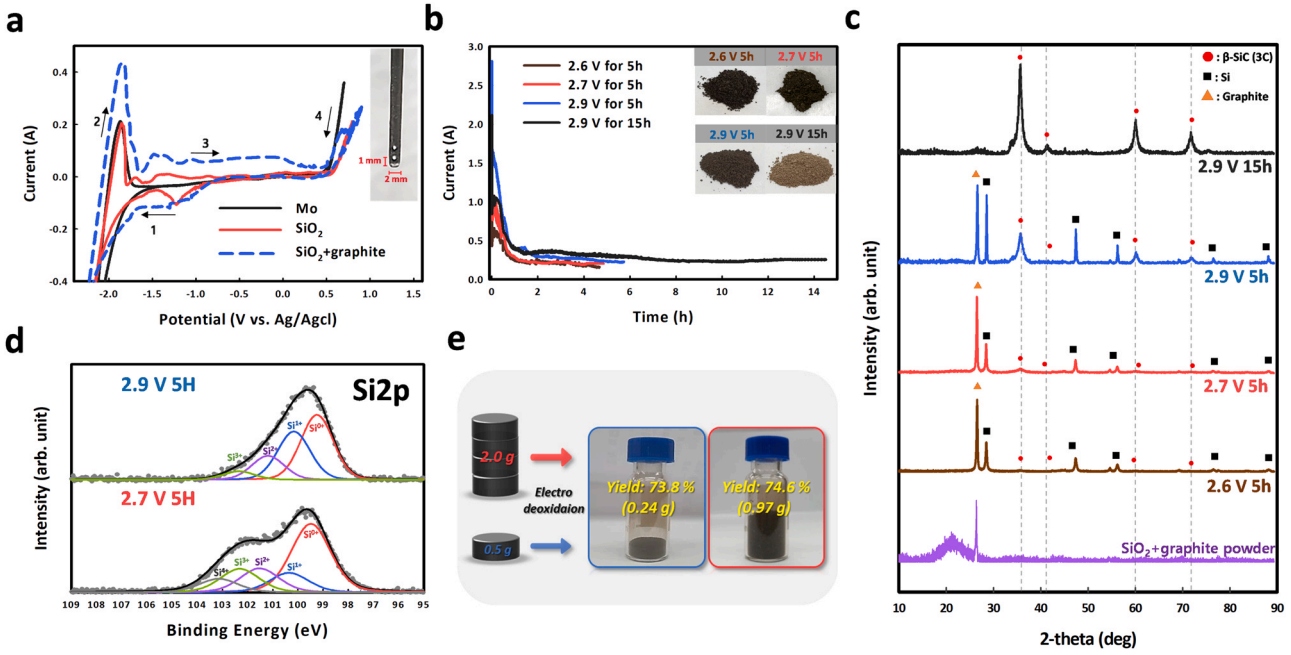

Fig. 2. Electro-deoxidation behaviour and structural characteristics of the SiO_2/graphite pellet and synthesised composite materials. (a) Cyclic voltammetry curves obtained for bare Mo metallic cavity electrode, SiO_2, and SiO_2/graphite electrodes at applied voltages between −2.4 and 0.8 V. (b) Time–current plots for the SiO_2/graphite pellet with inset photographs of the samples reduced under various electrolytic conditions. (c) X-ray diffraction and (d) Si 2p of the X-ray photoelectron spectroscopy patterns of SiO_2/graphite and the synthesised composite materials obtained under various electrolytic conditions. (e) Production yields of the Si@graphite@SiC composite obtained from the SiO_2/graphite pellets with weights of 0.5 and 2.0 g.

electrolytic reduction is the main cause of the observed reduction in the direct electrolysis yield. As shown in Fig. 2e, although several pellets are stacked vertically, this does not significantly decrease their contact area with the molten salt; hence, this setup can be structurally stabilised to produce similar yields during scaled-up syntheses. Therefore, the reaction yield increases owing to the high electrical conductivity of graphite, and its gram-scale values can be easily obtained by stacking pellets with various weights (Fig. S3). Notably, the peak at 102.4 eV is not detected in the sample produced at a voltage of 2.9 V and reaction time of 5 h due to Si oxidation.

Fig. 3 shows the morphological changes in the SiO_2/graphite pellets under various electro-deoxidation conditions. The composites produced by electro-deoxidation at different cell voltages and electrolysis times are presented in Fig. 3a–d. At a relatively low cell voltage (2.6 V; 5 h), the produced Si was located between the cracks of the exfoliated graphite (ex-graphite) layer (Fig. 3a), whereas at voltages of 2.7 and 2.9 V and a reaction time of 5 h, composites containing graphite, Si NWs, and SiC NWs were formed. When the electro-deoxidation was performed at a voltage of 2.9 V for 15 h, pure SiC NWs were produced, as shown in Fig. 3d. The SEM images of the four composites obtained at different cell voltages and electrolysis times correspond to the morphological changes that occur as the electrochemical reaction progresses (see also Fig. S4).

Fig. 3e–n shows the TEM images, HRTEM images, and selected area electron diffraction (SAED) patterns of the Si@graphite@SiC composites obtained at voltages of 2.7 and 2.9 V and a reaction time of 5 h. These composites were well-mixed, as evident from Fig. 3e and j. Fig. 3e demonstrates that the composite produced at 2.7 V contained a larger amount of Si owing to the relatively low cell voltage, because of which the produced Si NWs were several tens of nanometres in diameter. The HRTEM image in Fig. 3i depicts the D-spacing of the Si(111) crystalline plane, and the SAED pattern in Fig. 3 h represents the Si(111), Si(220), and Si(311) crystalline planes (this can also be seen in the EDS element mapping images of the Si NWs in Fig. S4f). The composite produced at the higher cell voltage (2.9 V) comprised a larger number of NWs (Fig. 3j) because of the effect of the SiC NWs formed at the relatively high cell voltage. The D-spacings of the Si crystalline and SiC(111) planes were determined simultaneously because the graphite and Si species, generated via electro-deoxidation, reacted to produce SiC (similar results are shown in the SAED pattern depicted in Fig. 3 m). TEM images of the sample obtained at a voltage of 2.6 V and an electrolysis time of 5 h are shown in Fig. S5a and b. The sample contained Si particles located between ex-graphite layers; however, it did not contain Si or SiC NWs. In addition, Fig. S5c and d shows the TEM images of the samples subjected to electro-deoxidation at a voltage of 2.9 V and reaction time of 15 h.

According to the morphological analyses performed in the present and other works, the deoxidation process of SiO_2/graphite composites can be described as follows: (1) When a negative potential is applied across the electrodes, the SiO_2 layer around the Ni wire, used as the current lead, is first reduced to Si, owing to the chemical potential difference. (2) The reduction of the produced Si generates vertical cracks, which facilitate $CaCl_2$ penetration. (3) The reduced Si acts as a conductor at high temperatures, and the SiO_2 species that form along the cracks into which $CaCl_2$ penetrates are subjected to a continuous reduction reaction along with the initially produced Si, leading to the formation of Si NWs [43]. (4). Steps (2) and (3) repeat to continuously produce Si NWs. (5) Finally, the Si NWs react with the adjacent graphite layers to generate SiC NWs [35].

The production of ex-graphite facilitates intense deoxidation of the adjacent SiO_2 species, and Ca^{2+} ions penetrate the graphite layers during cathodic polarisation. This phenomenon can be explained by considering the electro-deoxidation of graphite pellets (Fig. S6). Unlike the pellets soaked in molten $CaCl_2$ salt for 10 h, those undergoing electro-deoxidation exhibited disorderly split shapes. Therefore, the ex-graphite, produced by electro-deoxidation, can effectively control the volume expansion of Si particles along with Si and SiC NWs, and thus improve the performance of cathode materials.

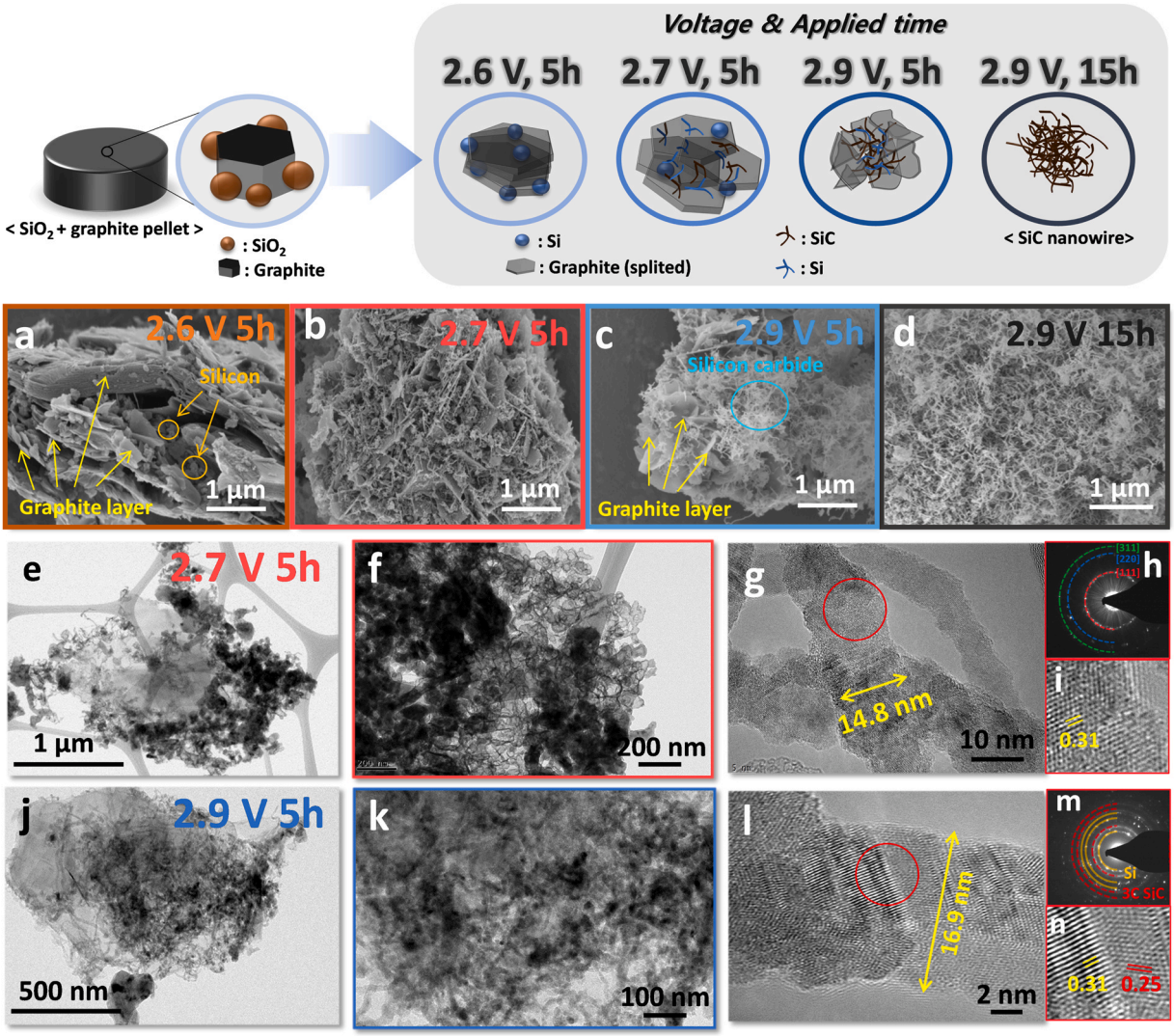

Fig. 3. Morphologies of the composite materials prepared by electro-deoxidation. (a)–(d) Scanning electron microscopy images of the composites synthesised at different voltages (2.6, 2.7, or 2.9 V) and electrolysis times (5 or 15 h). (e)–(i) Composite synthesised at a voltage of 2.7 V for 5 h: (e), (f) Transmission electron microscopy (TEM) images; (g) High resolution transmission electron microscopy (HRTEM) image; (h) Selected area electron diffraction (SAED) pattern; and (i) atomic-resolution HRTEM. (j)–(n) Composite synthesised at a voltage of 2.9 V for 5 h: (j), (k) TEM images; (l) HRTEM images; (m) SAED pattern; and (n) atomic-resolution HRTEM image.

The composites produced at various cell voltages and electrolysis times were used in half-cells for GCD testing to determine the optimal manufacturing conditions for energy storage applications. Fig. 4a shows the first GCD curves of the samples produced under different conditions. The voltage plateau below 0.1 V indicates the lithiation of graphite and Si species, whose delithiation occurs near 0.15 and 0.4 V, respectively. The composite fabricated at a voltage of 2.6 V and reaction time of 5 h had the highest initial discharge capacity of 1610 mAh g^{-1} and CE of 75.9%, followed by the samples manufactured at 2.7 V for 5 h, 2.9 V for 5 h, and 2.9 V for 15 h, which possessed initial discharge capacities of 836, 688, and 269 mAh g^{-1} and CEs of 76.5%, 75.7%, and 68.5%, respectively. Fig. S7 shows the dQ/dV curves of the samples produced under different conditions, which results are reflected in the voltage profile in Fig. 4a. The cathodic peak detected near 0.1 V corresponds to the Si–Li alloying process, and the anodic peaks at 0.15 and 0.4 V originate from the delithiation of graphite and Si, respectively. As the SiC contents increased, the reaction voltage region of graphite and Si shifted and gradually disappeared.

Fig. 4b depicts the d*Q*/d*V* curve constructed for studying the electrochemical reaction of the (2.9 V, 5 h) sample with Li^+. The cathodic and anodic peaks match the voltage plateaus shown in Fig. 4a, and the composites exhibiting slight peak shifts during the 1st, 50th, and 100th cycles possess high electrochemical reversibility. Notably, no oxidation–reduction peak, resulting from the electrochemical reaction of SiC, was observed for any composite, as SiC was not involved in the lithiation process.

The SiC NWs in the composite structure act as an active matrix that accommodates Si volume expansion and consequently enhances the electrode cyclability. Therefore, the higher the SiC content and lower the electrode capacity, the higher the rate capability and cyclability, as shown in Fig. 4c–e. Fig. 4c displays the relatively high lithiation capacities and capacity retention corresponding to a rate capability of 31.8% at specific currents of 200–6000 mA g^{-1} without SiC formation. Increasing the SiC content decreases the electrode capacity and increases the rate capability. The samples fabricated at 2.7 V for 5 h (red) and at 2.9 V for 5 h (blue) demonstrated high rate capabilities of 43.7% and 44.2%, respectively, in the specific current range of 200–6000 mA g^{-1}. In addition, all samples exhibited excellent capacity recovery rates, even at a current of 200 mA g^{-1}, owing to the high electrical conductivity of the graphite phase.

Fig. 4d compares the cyclabilities of the different composites over 150 cycles. The sample fabricated at 2.6 V for 5 h (brown) exhibits a

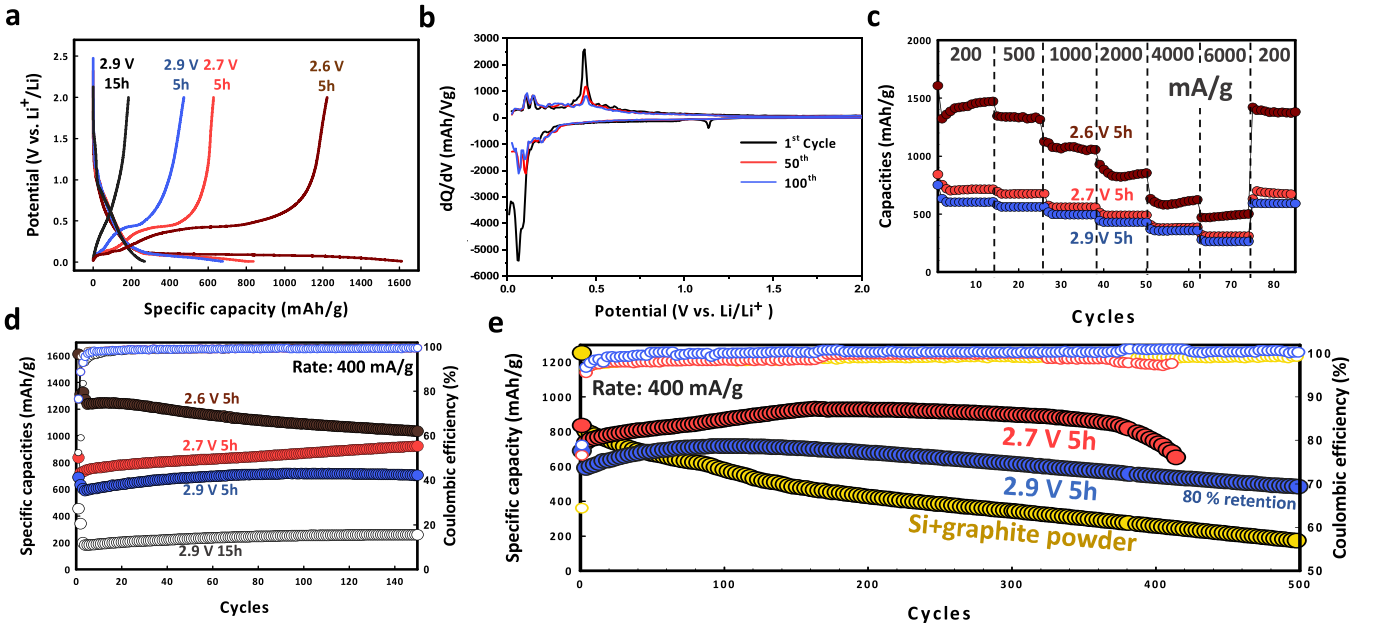

Fig. 4. Electrochemical characterisation of the fabricated Si@graphite@SiC anode materials. (a) Charge–discharge curves and (b) dQ/dV profiles in the potential range of 0.01–2.0 V vs. Li^+/Li of the electrode prepared at a voltage of 2.9 V and electrolysis time of 5 h. (c) Lithiation/delithiation capacities determined in the current range of 200–6000 mA g^{-1} (the first two cycles were performed at a specific current of 100 mA g^{-1}). (d) Cycling performance of the Si@graphite@SiC samples and (e) comparison with a commercially available Si/graphite powder mixture.

capacity retention of 83.6%, whereas the other composites show good cyclabilities with a small capacity decrease. In addition, Fig. S8 shows the long-term capacity retention of the 2.6 V–5 h sample. The result shows 1326 mAh g^{-1} after the second cycle, and a capacity retention rate of 62.9% is observed with 835 mAh g^{-1} after 390 cycles. However, the composite fabricated at 2.9 V for 15 h (white), which consists of pure SiC, demonstrates relatively low capacity and CE. Among the various samples, the cyclabilities of the composites prepared at 2.7 and 2.9 V for 5 h were superior to those of the Si/graphite mixture (Fig. 4e) owing to the formation of ex-graphite, Si NWs, and SiC NWs during the electro-deoxidation. Here, the ex-graphite phase increases the electrical conductivity of the composite and accommodates its volume expansion, whereas the Si NWs exhibit better electrochemical performance than the conventional Si particles, as reported previously [5]. Although SiC NWs have a lower reactivity towards Li^+ (Fig. 4b), SiC acts as an active matrix that accommodates Si electrode expansion during the electrochemical reaction, which increases the cycle life of the composite electrode [44]. The observed capacity increase during the initial charge–discharge cycles is due to the initially high surface area of ex-graphite, which subsequently decreases owing to Li^+ insertion during the lithiation process.

The areal capacity of an electrode is an important factor affecting the miniaturisation and lightweight nature of batteries. However, thick electrodes are difficult to manufacture due to the electrolyte loss caused by the negative side-reactions during the charging period, long electron transfer channels, and high equivalent series resistance. As a result, previous studies on Si-based electrodes have focussed on increasing their cyclability by varying the mass loading of the active material [45]. In order to evaluate the electrochemical properties of the electrode with a high mass loading, the prepared Si@graphite@SiC composite was subjected to GCD tests at mass loadings of 0.73–3.5 mg cm^{-2}.

The first GCD curve depicted in Fig. 5a exhibits an identical lithiation/delithiation plateau, as compared to that obtained at a high mass loading (Fig. 4a), suggesting that stable electron transfer occurred due to the high electrical conductivity and mechanical stability of the electrodes. The electrode fabricated at 2.7 V for 5 h exhibited a large initial discharge capacity of 4.6 mAh cm^{-2} relative to the loading amount, which exceeds the values obtained for other reported Si–C composite electrodes (Fig. S9).

Fig. 5b and c shows the areal capacities of the composite materials with different mass loadings. The active loading of the samples produced at 2.7 and 2.9 V for 5 h increased to approximately 3.5 mg cm^{-2}, which corresponded to a linear increase in the areal capacity (Fig. S10). Therefore, this indicates that the electron transfer was successful even within the thick electrode with a high mass loading. The composite electrode fabricated at 2.7 V for 5 h exhibited a high areal capacity at 3.49 mg cm^{-2} (Fig. 5b); however, its capacity slightly decreased during cycling. After 36 cycles, a new Li cathode was installed to prevent the decomposition of Li due to excessive reactions [45]; nevertheless, a continuous capacity reduction corresponding to a capacity retention of 75.1% was observed.

Moreover, the composite electrode produced at 2.9 V for 5 h (Fig. 5c) demonstrated excellent cycle life at a mass loading of 3.51 g cm^{-2}, capacity retention of 89.4%, and high average CE over the initial 10–50 cycles (Fig. 5d). Both compounds possessed relatively low CEs combined with some capacity reduction at a loading of 3.5 mg cm^{-2} and higher, indicating that the active mass loading limit of the complex electrode is equal to approximately 3.5 mg cm^{-2}. The areal capacity of commercial Si-based materials is 3.0 mAh cm^{-2} or greater. High-areal-capacity materials can minimise the use of inactive materials, such as current collector and separator, achieve maximum volumetric and gravimetric energy densities, and lower the overall battery cost. Hence, the prepared Si@graphite@SiC composite (at 2.9 V for 5 h) is suitable for manufacturing commercial anode materials with high areal capacities, good cyclability, and high average CEs.

To further evaluate the feasibility of using Si@graphite@SiC electrodes in LIBs, a full cell was assembled using a commercial NCM622 cathode and the Si@graphite@SiC anode. The electrode fabricated at 2.9 V for 5 h was selected, as it exhibited the highest CE among the fabricated compounds. A typical charge–discharge curve of the Si@graphite@SiC/NCM full cell is shown in Fig. 5e. The full cell exhibited a high reversible capacity of 130 mAh g^{-1} at a specific current of 0.1 C with a capacity retention of 84% for over 70 cycles.

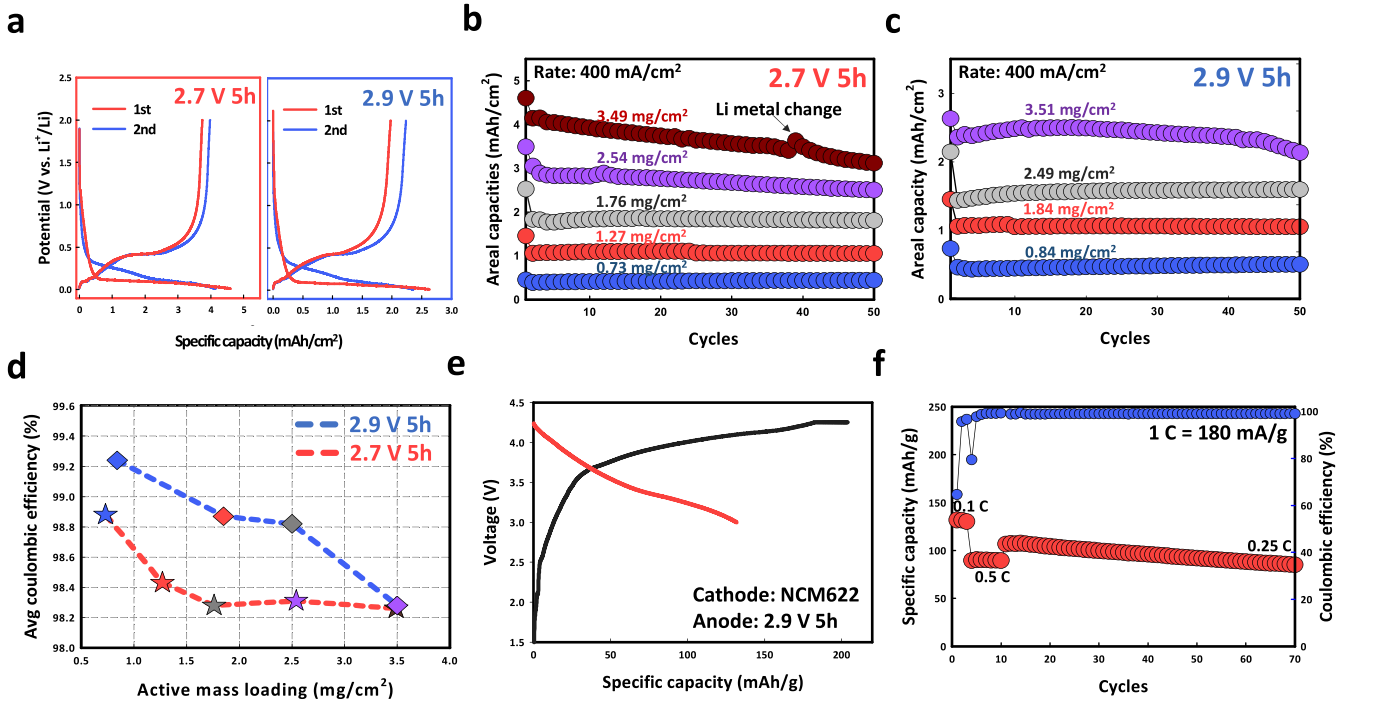

Fig. 5. Electrochemical characterisation of the Si@graphite@SiC anode materials. (a) Charge–discharge curves recorded for the electrodes with active loadings of 3.49 and 3.51 mg cm^{-2}. These electrodes were fabricated at an electrolysis time of 5 h and voltages of 2.7 and 2.9 V, respectively. (b), (c) Cycling stabilities and (d) Coulombic efficiencies (%) of the thick electrodes that were fabricated at voltages of 2.7 and 2.9 V and for electrolysis time of 5 h with various active loadings. (e) Charge–discharge curves and (f) rate performance of the full cell, with the Si@graphite@SiC anode and NCM622 cathode, determined at specific currents of 0.1–0.25 C (1 C = 180 mA g^{-1}).

Moreover, the full cell exhibited a high rate capability of 112 mAh g^{-1} at 0.25 C, as shown in Fig. 5 f.

4. Conclusion

In this study, we proposed a novel Si@graphite@SiC anode material with high electrochemical performance for LIBs. Through molten salt electrolysis, Si NWs were grown in situ on ex-graphite via SiC connections, which was confirmed by XRD, XPS, and TEM–EDS. The prepared Si@graphite@SiC composite exhibited a high areal capacity of 4.6 mAh cm^{-2} and good cyclability during half-cell tests. Moreover, the full cell, containing the prepared composite anode and commercial cathode, demonstrated high capacity with good capacity retention of 84% after 70 cycles. This work provides new insights into the rational design of alloy anodes for high-energy batteries. In addition, the findings suggest that the Si@graphite@SiC composite can be applied in LIBs, especially those undergoing large volume changes during operation, and advanced electrochemical energy storage devices.

CRediT authorship contribution statement

J.-H.C., **H.-K.K.**, and **S.M.J.** designed the materials and experiments. **J.-H.C.** fabricated the materials. **J.-H.C.** and **S. C.** performed the electrochemical characterisation. **S.C.**, and **J.S.C.** participated in the electrochemical evaluations and structural characterisation. **H.-K.K.** and **J.-H.C.** wrote the manuscript. **H.-K.K.**, and **S.M.J.** reviewed the manuscript. All authors discussed the results and commented on the manuscript. All authors have given approval to the final version of the manuscript.

Declaration of Competing Interest

The authors declare that they have no known competing financial interests or personal relationships that could have appeared to influence the work reported in this paper.

Acknowledgements

This work was supported by the National Research Foundation of Korea (NRF) grant funded by the Korea Government (MSIT) (No. 2019R1A2C1086075, No. 2021R1F1A1059139) and by the Korea Evaluation Institute of Industrial Technology (KEIT) funded by the Korea Government (MOTIE) (No. 20010551).

Appendix A. Supporting information

Supplementary data associated with this article can be found in the online version at doi:10.1016/j.jallcom.2021.163010.

References

[1] J.R. Dahn, T. Zheng, Y. Liu, J.S. Xue, Mechanisms for lithium insertion in carbonaceous materials, Science 270 (1995) 590–593, https://doi.org/10.1126/science.270.5236.590

[2] M.S. Javed, S.S.A. Shah, T. Najam, S.H. Siyal, S. Hussain, M. Saleem, Z. Zhao, W. Mai, Achieving high-energy density and superior cyclic stability in flexible and lightweight pseudocapacitor through synergic effects of binder-free $CoGa_2O_4$ 2D-hexagonal nanoplates, Nano Energy 77 (2020) 105276, https://doi.org/10.1016/j.nanoen.2020.105276

[3] M.S. Javed, H. Lei, Z. Wang, B.-T. Liu, X. Cai, W. Mai, 2D V_2O_5 nanosheets as a binder-free high-energy cathode for ultrafast aqueous and flexible Zn-ion batteries, Nano Energy 70 (2020) 104573, https://doi.org/10.1016/j.nanoen.2020.104573

[4] M.S. Javed, N. Shaheen, S. Hussain, J. Li, S.S.A. Shah, Y. Abbas, M.A. Ahmad, R. Raza, W. Mai, An ultra-high energy density flexible asymmetric supercapacitor based on hierarchical fabric decorated with 2D bimetallic oxide nanosheets and MOF-derived porous carbon polyhedral, J. Mater. Chem. A 7 (2019) 946–957, https://doi.org/10.1039/C8TA08816K

[5] M.S. Javed, S. Dai, M. Wang, D. Guo, L. Chen, X. Wang, C. Hu, Y. Xi, High performance solid state flexible supercapacitor based on molybdenum sulfide hierarchical nanospheres, J. Power Sources 285 (2015) 63–69, https://doi.org/10.1016/j.jpowsour.2015.03.079

[6] M.T. McDowell, S.W. Lee, W.D. Nix, Y. Cui, 25th anniversary article: understanding the lithiation of silicon and other alloying anodes for lithium-ion batteries, Adv. Mater. 25 (2013) 4966–4985, https://doi.org/10.1002/adma.201301795

[7] L.Y. Beaulieu, K.W. Eberman, R.L. Turner, L.J. Krause, J.R. Dahn, Colossal reversible volume changes in lithium alloys, Electrochem. Solid-State Lett. 4 (2001) A137, https://doi.org/10.1149/1.1388178

[8] U. Kasavajjula, C. Wang, A.J. Appleby, Nano-and bulk-silicon-based insertion anodes for lithium-ion secondary cells, J. Power Sources 163 (2007) 1003–1039, https://doi.org/10.1016/j.jpowsour.2006.09.084

[9] C.K. Chan, H. Peng, G. Liu, K. Mcllwrath, X.F. Zhang, R.A. Huggins, Y. Cui, High-performance lithium battery anodes using silicon nanowires, Nat. Nanotechnol. 3 (2008) 31–35, https://doi.org/10.1038/nnano.2007.411

[10] M. Gauthier, D. Mazouzi, D. Reyter, B. Lestriez, P. Moreau, D. Guyomard, L. Roue, A low-cost and high performance ball-milled Si-based negative electrode for high-energy Li-ion batteries, Energy Environ. Sci. 6 (2013) 2145–2155, https://doi.org/10.1039/C3EE41318G

[11] M. Ge, J. Rong, X. Fang, C. Zhou, Porous doped silicon nanowires for lithium ion battery anode with long cycle life, Nano Lett. 12 (2012) 2318–2323, https://doi.org/10.1021/nl300206e

[12] Y. Yao, M.T. McDowell, I. Ryu, H. Wu, N. Liu, L. Hu, W.D. Nix, Y. Cui, Interconnected silicon hollow nanospheres for lithium-ion battery anodes with long cycle life, Nano Lett. 11 (2011) 2949–2954, https://doi.org/10.1021/nl201470j

[13] E. Park, J. Kim, D.J. Chung, M.-S. Park, H. Kim, J.H. Kim, Si/SiO_x-conductive polymer core-shell nanospheres with an improved conducting path preservation for lithium-ion battery, ChemSusChem 9 (2016) 2754–2758, https://doi.org/10.1002/cssc.201600798

[14] N. Liu, Z. Lu, J. Zhao, M.T. McDowell, H.W. Lee, W. Zhao, Y. Cui, A pomegranate-inspired nanoscale design for large-volume-change lithium battery anodes, Nat. Nanotechnol. 9 (2014) 187–192, https://doi.org/10.1038/nnano.2014.6

[15] D. Lin, Z. Lu, P.-C. Hsu, H.R. Lee, N. Liu, J. Zhao, H. Wang, C. Liu, Y. Cui, A high tap density secondary silicon particle anode fabricated by scalable mechanical pressing for lithium-ion batteries, Energy Environ. Sci. 8 (2015) 2371–2376, https://doi.org/10.1039/C5EE01363A

[16] P. Li, J.-Y. Hwang, Y.-K. Sun, Nano/microstructured silicon–graphite composite anode for high-energy-density Li-ion battery, ACS Nano 13 (2019) 2624–2633, https://doi.org/10.1021/acsnano.9b00169

[17] J.-H. Choi, H.-K. Kim, E.-M. Jin, M.W. Seo, J.S. Cho, R.V. Kumar, S.M. Jeong, Facile and scalable synthesis of silicon nanowires from waste rice husk silica by the molten salt process, J. Hazard. Mater. 399 (2020) 122949, https://doi.org/10.1016/j.jhazmat.2020.122949

[18] W. Luo, X. Chen, Y. Xia, M. Chen, L. Wang, Q. Wang, W. Li, J. Yang, Surface and interface engineering of silicon-based anode materials for lithium-ion batteries, Adv. Energy Mater. 7 (2017) 1701083, https://doi.org/10.1002/aenm.201701083

[19] L.-F. Cui, L. Hu, J.W. Choi, Y. Cui, Light-weight free-standing carbon nanotube-silicon films for anodes of lithium ion batteries, ACS Nano 4 (2010) 3671–3678, https://doi.org/10.1021/nn100619m

[20] I.H. Son, J.H. Park, S. Kwon, S. Park, M.H. Rümmeli, A. Bachmatiuk, H.J. Song, J. Ku, J.W. Choi, J.-M. Choi, S.-G. Doo, H. Chang, Silicon carbide-free graphene growth on silicon for lithium-ion battery with high volumetric energy density, Nat. Commun. 6 (2015) 1–8, https://doi.org/10.1038/ncomms8393

[21] T.H. Hwang, Y.M. Lee, B.-S. Kong, J.-S. Seo, J.W. Choi, Electrospun core–shell fibers for robust silicon nanoparticle-based lithium ion battery anodes, Nano Lett. 12 (2012) 802–807, https://doi.org/10.1021/nl203817r

[22] T. Kasukabe, H. Nishihara, K. Kimura, T. Matsumoto, H. Kobayashi, M. Okai, T. Kyotani, Beads-milling of waste Si sawdust into high-performance nanoflakes for lithium-ion batteries, Sci. Rep. 7 (2017) 42734, https://doi.org/10.1038/srep42734

[23] S. Choi, D.S. Jung, J.W. Choi, Scalable fracture-free SiOC glass coating for robust silicon nanoparticle anodes in lithium secondary batteries, Nano Lett. 14 (2014) 7120–7125, https://doi.org/10.1021/nl503620z

[24] S.-H. Park, H.-K. Kim, S.-B. Yoon, C.-W. Lee, D. Ahn, S.-I. Lee, K.C. Roh, K.-B. Kim, Spray-assisted deep-frying process for the in situ spherical assembly of graphene for energy-storage devices, Chem. Mater. 27 (2015) 457–465, https://doi.org/10.1021/cm5034244

[25] C. Xu, B. Wang, H. Luo, P. Jing, X. Zhang, Q. Wang, Y. Zhang, H. Wu, Embedding silicon in pinecone-derived porous carbon as a high-performance anode for lithium-ion batteries, ChemElectroChem 7 (2020) 2889–2895, https://doi.org/10.1002/celc.202000827

[26] H.J. Kwon, J.Y. Hwang, H.J. Shin, M.G. Jeong, K.Y. Chung, Y.K. Sun, H.G. Jung, Nano/microstructured silicon-carbon hybrid composite particles fabricated with corn starch biowaste as anode materials for Li-ion batteries, Nano Lett. 20 (2020) 625–635, https://doi.org/10.1021/acs.nanolett.9b04395

[27] A.R. Kamali, H.-K. Kim, K.-B. Kim, R.V. Kumar, D.J. Fray, Large scale green production of ultra-high capacity anode consisting of graphene encapsulated silicon nanoparticles, J. Mater. Chem. A 5 (2017) 19126–19135, https://doi.org/10.1039/C7TA04335J

[28] Y.-C. Zhang, Y. You, S. Xin, Y.-X. Yin, J. Zhang, P. Wang, X.-S. Zheng, F.-F. Cao, Y.-G. Guo, Rice husk-derived hierarchical silicon/nitrogen-doped carbon/carbon nanotube spheres as low-cost and high-capacity anodes for lithium-ion batteries, Nano Energy 25 (2016) 120–127, https://doi.org/10.1016/j.nanoen.2016.04.043

[29] X. Shen, Z. Tian, R. Fan, L. Shao, D. Zhang, G. Cao, L. Kou, Y. Bai, Research progress on silicon/carbon composite anode materials for lithium-ion battery, J. Energy Chem. 27 (2018) 1067–1090, https://doi.org/10.1016/j.jechem.2017.12.012

[30] K.S. Mohandas, D.J. Fray, FFC Cambridge process and removal of oxygen from metal-oxygen systems by molten salt electrolysis: an overview, Trans. Indian Inst. Met. 57 (2004) 579–592.

[31] T. Nohira, K. Yasuda, Y. Ito, Pinpoint and bulk electrochemical reduction of insulating silicon dioxide to silicon, Nat. Mater. 2 (2003) 397–401, https://doi.org/10.1038/nmat900

[32] S. Lu, J. Yang, X. Wang, H. Ding, Z. Gao , (China Automotive Battery Research Institute Co., Ltd.), Nano Silicon-carbon Composite Material and Preparation Method Thereof, US Pat. 9666863, 2017.

[33] X. Zou, L. Ji, X. Lu, Z. Zhou, Facile electrosynthesis of silicon carbide nanowires from silica/carbon precursors in molten salt, Sci. Rep. 7 (2017) 9978, https://doi.org/10.1038/s41598-017-10587-5

[34] D.S.M. Vishnu, J. Sure, H.-K. Kim, R.V. Kumar, C. Schwandt, Solid state electrochemically synthesised β-SiC nanowires as the anode material in lithium ion batteries, Energy Storage Mater. 26 (2020) 234–241, https://doi.org/10.1016/j.ensm.2019.12.041

[35] D.S.M. Vishnu, J. Sure, H.-K. Kim, J.Y. Kim, R.V. Kumar, C. Schwandt, Direct electrochemical preparation of nanostructured silicon carbide and its nitridation behavior, J. Electrochem. Soc. 165 (2018) D731–D742, https://doi.org/10.1149/2.0591814jes

[36] Z. Zhao, H. Xie, J. Qu, H. Zhao, Q. Ma, P. Xing, Q. Song, D. Wang, H. Yin, A natural transporter of silicon and carbon: conversion of rice husks to silicon carbide or carbon-silicon hybrid for lithium-ion battery anodes via a molten salt electrolysis approach, Batter. Supercaps 2 (2019) 1007–1015, https://doi.org/10.1002/batt.201900091

[37] Z. Yu, S. Fang, N. Wang, B. Shi, Y. Hu, Z. Shi, D. Shi, J. Yang, In-situ growth of silicon nanowires on graphite by molten salt electrolysis for high performance lithium-ion batteries, Mater. Lett. 273 (2020) 127946, https://doi.org/10.1016/j.matlet.2020.127946

[38] Y. Hu, B. Yu, X. Qi, B. Shi, S. Fang, Z. Yu, J. Yang, The preparation of graphite/silicon@ carbon composites for lithium-ion batteries through molten salts electrolysis, J. Mater. Sci. 55 (2020) 10155–10167, https://doi.org/10.1007/s10853-020-04756-7

[39] Z. Wang, Y. Li, S. Huang, L. Liu, Y. Wang, J. Jin, D. Kong, L. Zhang, O.G. Schmidt, PVD customized 2D porous amorphous silicon nanoflakes percolated with carbon nanotubes for high areal capacity lithium ion batteries, J. Mater. Chem. A 8 (2020) 4836–4843, https://doi.org/10.1039/c9ta12923e

[40] M. Furquan, M.K. Jangid, A.R. Khatribail, S. Vijayalakshmi, A. Mukhopadhyay, S. Mitra, Mechanical and electrochemical stability improvement of sic-reinforced silicon-based composite anode for Li-ion batteries, ACS Appl. Energy Mater. 3 (2020) 12613–12626, https://doi.org/10.1021/acsaem.0c02523

[41] H.S. Ji, H.Y. Ryu, E.Y. Choi, S.W. Cho, M.F. Simpson, S.M. Jeong, Preparation of NdNi5 using an electrochemical reduction of a NiO–Nd_2O_3 mixture in molten LiCl, J. Ind. Eng. Chem. 24 (2015) 259–265, https://doi.org/10.1016/j.jiec.2014.09.039

[42] M.S. Chandrasekar, N.R. Srinivasan, Role of SiO_x on the photoluminescence properties of β-SiC, Ceram. Int. 42 (2016) 8900–8908, https://doi.org/10.1016/j.ceramint.2016.02.145

[43] K. Yasuda, T. Nohira, K. Amezawa, Y.H. Ogata, Y. Ito, Mechanism of direct electrolytic reduction of solid SiO2 to Si in molten CaCl2, J. Electrochem. Soc. 152 (2005) D69, https://doi.org/10.1149/1.1864453

[44] I.-S. Kim, G.E. Blomgren, P.N. Kumta, Si–SiC nanocomposite anodes synthesized using high-energy mechanical milling, J. Power Sources 130 (2004) 275–280, https://doi.org/10.1016/j.jpowsour.2003.12.014

[45] S. Choi, T.-W. Kwon, A. Coskun, J.W. Choi, Highly elastic binders integrating polyrotaxanes for silicon microparticle anodes in lithium ion batteries, Science 357 (2017) 279–283, https://doi.org/10.1126/science.aal4373